

MICROLENSING TOWARDS THE LMC

PHILIPPE JETZER

*Institute of Theoretical Physics, University of Zürich, Winterthurerstrasse 190, CH-8057
Zürich, Switzerland
E-mail: jetzer@physik.unizh.ch*

The nature and the location of the lenses discovered in the microlensing surveys done so far towards the LMC remain unclear. Motivated by these questions we computed the optical depth for the different intervening populations and the number of expected events for self-lensing, using a recently drawn coherent picture of the geometrical structure and dynamics of the LMC. By comparing the theoretical quantities with the values of the observed events it is possible to put some constraints on the location and the nature of the MACHOs. Clearly, given the large uncertainties and the few events at disposal it is not yet possible to draw sharp conclusions, nevertheless we find that up to 3-4 MACHO events might be due to lenses in LMC, which are most probably low mass stars, but that hardly all events can be due to self-lensing. The most plausible solution is that the events observed so far are due to lenses belonging to different intervening populations: low mass stars in the LMC, in the thick disk, in the spheroid and some true MACHOs in the halo of the Milky Way and the LMC itself.

1. Introduction

The location and the nature of the microlensing events found so far towards the Large Magellanic Cloud (LMC) is still a matter of controversy. The MACHO collaboration found 13 to 17 events in 5.7 years of observations, with a mass for the lenses estimated to be in the range $0.15 - 0.9 M_{\odot}$ assuming a standard spherical Galactic halo¹ and derived an optical depth of $\tau = 1.2_{-0.3}^{+0.4} \times 10^{-7}$. The EROS2 collaboration² announced the discovery of 4 events based on three years of observation but monitoring about twice as much stars as the MACHO collaboration. The MACHO collaboration monitored primarily 15 deg^2 in the central part of the LMC, whereas the EROS2 experiment covers a larger solid angle of 64 deg^2 but in less crowded fields. The EROS2 microlensing rate should thus be less affected by self-lensing. This might be the reason for the fewer events seen by EROS2 as compared to the MACHO experiment.

The hypothesis for a self-lensing component was discussed by several authors 3,4,5,6. The analysis of Jetzer et al. ⁷ and Mancini et al. ⁸ has shown that probably the observed events are distributed among different galactic components (disk, spheroid, galactic halo, LMC halo and self-lensing). This means that the lenses do not belong all to the same population and their astrophysical features can

differ deeply one another.

Some of the events found by the MACHO team are most probably due to self-lensing: the event MACHO-LMC-9 is a double lens with caustic crossing⁹ and its proper motion is very low, thus favouring an interpretation as a double lens within the LMC. The source star for the event MACHO-LMC-14 is double¹⁰ and this has allowed to conclude that the lens is most probably in the LMC. The expected LMC self-lensing optical depth due to these two events has been estimated to lie within the range¹⁰ $1.1 - 1.8 \times 10^{-8}$, which is still below the expected optical depth for self-lensing even when considering models giving low values for the optical depth. The event LMC-5 is due to a disk lens¹¹ and indeed the lens has even been observed with the HST. The other stars which have been microlensed were also observed but no lens could be detected, thus implying that the lens cannot be a disk star but has to be either a true halo object or a faint star or brown dwarf in the LMC itself.

Thus up to now the question of the location of the observed MACHO events is unsolved and still subject to discussion. Clearly, with much more events at disposal one might solve this problem by looking for instance at their spatial distribution. To this end a correct knowledge of the structure and dynamics of the luminous part of the LMC is essential, and we take advantage of the new picture drawn by van der Marel et al. ^{12,13,14}.

2. LMC model

In a series of three interesting papers ^{12,13,14}, a new coherent picture of the geometrical structure and dynamics of LMC has been given. In the following we adopt this model and use the same coordinate systems and notations as in van der Marel. We consider an elliptical isothermal flared disk tipped by an angle $i = 34.7^\circ \pm 6.2^\circ$ as to the sky plane, with the closest part in the north-east side. The center of the disk coincides with the center of the bar and its distance from us is $D_0 = 50.1 \pm 2.5$ kpc. We take a bar mass $M_{\text{bar}} = 1/5 M_{\text{disk}}$ with $M_{\text{bar}} + M_{\text{disk}} = M_{\text{vis}} = 2.7 \times 10^9 M_\odot$.

The vertical distribution of stars in an isothermal disk is described by the sech^2 function; therefore the spatial density of the disk is modeled by:

$$\rho_d = \frac{N M_d}{4\pi q R_d^2 \zeta_d(0)} \text{sech}^2 \left(\frac{\zeta}{\zeta_d(R)} \right) e^{-\frac{1}{R_d} \sqrt{\left(\frac{\zeta}{q}\right)^2 + \eta^2}}, \quad (1)$$

where $q = 0.688$ is the ellipticity factor, $R_d = 1.54$ kpc is the scale length of the exponential disk, R is the radial distance from the center on the disk plane. $\zeta_d(R)$ is the *flaring* scale height, which rises from 0.27 kpc to 1.5 kpc at a distance of 5.5 kpc from the center¹⁴, and is given by

$$\zeta_d(R) = 0.27 + 1.40 \tanh \left(\frac{R}{4} \right) .$$

$N = 0.2765$ is a normalization factor that takes into account the flaring scale height.

In a first approach⁷ we have described the bar by a Gaussian density profile following Gyuk et al. ¹⁵, whereas in a following paper⁸ we choose, instead, a bar

spatial density that takes into account its boxy shape⁶:

$$\rho_b = \frac{2 M_b}{\pi^2 R_b^2 \Xi_b} e^{-\left(\frac{\Xi_b}{R_b}\right)^2} e^{-\frac{1}{R_b^4}(\gamma^2 + \zeta^2)^2}, \quad (2)$$

where $\Xi_b = 1.2$ kpc is the scale length of the bar axis, $R_b = 0.44$ kpc is the scale height along a circular section (for a more detailed discussion and definition of the coordinate system see ⁸).

The column density, projected on the $x - y$ sky plane is plotted in Fig. 1, giving a global view of the LMC shape for a terrestrial observer, together with the positions of the microlensing events detected by the MACHO (filled stars and empty diamonds) and EROS (filled triangles) collaborations, and the direction of the line of nodes. The maximum value of the column density, $41.5 \times 10^7 M_\odot \text{ kpc}^{-2}$, is assumed in the center of LMC.

We use two different models to describe the halo profile density: a spherical halo and an ellipsoidal halo. The values of the parameters have been chosen so that the models have roughly the same mass within the same radius. In the spherical model we neglect the tidal effects due to our Galaxy, and we adopt a classical pseudo-isothermal spherical density profile:

$$\rho_{h,S} = \rho_{0,S} \left(1 + \frac{R^2}{a^2}\right)^{-1} \theta(R_t - R), \quad (3)$$

where a is the LMC halo core radius, $\rho_{0,S}$ the central density, R_t a cutoff radius and θ the Heaviside step function. We use $a = 2$ kpc. We fix the value for the mass of the halo within a radius of 8.9 kpc equal to¹⁴ $5.5 \times 10^9 M_\odot$ that implies $\rho_{0,S}$ equal to $1.76 \times 10^7 M_\odot \text{ kpc}^{-3}$. Assuming a halo truncation radius¹⁴, $R_t = 15$ kpc, the total mass of the halo is $\approx 1.08 \times 10^{10} M_\odot$.

For the galactic halo we assume a spherical model with density profile given by:

$$\rho_{GH} = \rho_0 \frac{R_C^2 + R_S^2}{R_C^2 + R^2}, \quad (4)$$

where R is the distance from the galactic center, $R_C = 5.6$ kpc is the core radius, $R_S = 8.5$ kpc is the distance of the Sun from the galactic center and $\rho_0 = 7.9 \times 10^6 M_\odot \text{ kpc}^{-3}$ is the mass density in the solar neighbourhood.

3. Optical depth

The computation is made by weighting the optical depth with respect to the distribution of the source stars along the line of sight (see Eq.(7) in Jetzer et al. ⁷):

$$\tau = \frac{4\pi G}{c^2} \frac{\int_0^{\infty} \left[\int_0^{D_{os}} \frac{D_{ol}(D_{os} - D_{ol})}{D_{os}} \rho_1 dD_{ol} \right] \rho_s dD_{os}}{\int_0^{\infty} \rho_s dD_{os}}. \quad (5)$$

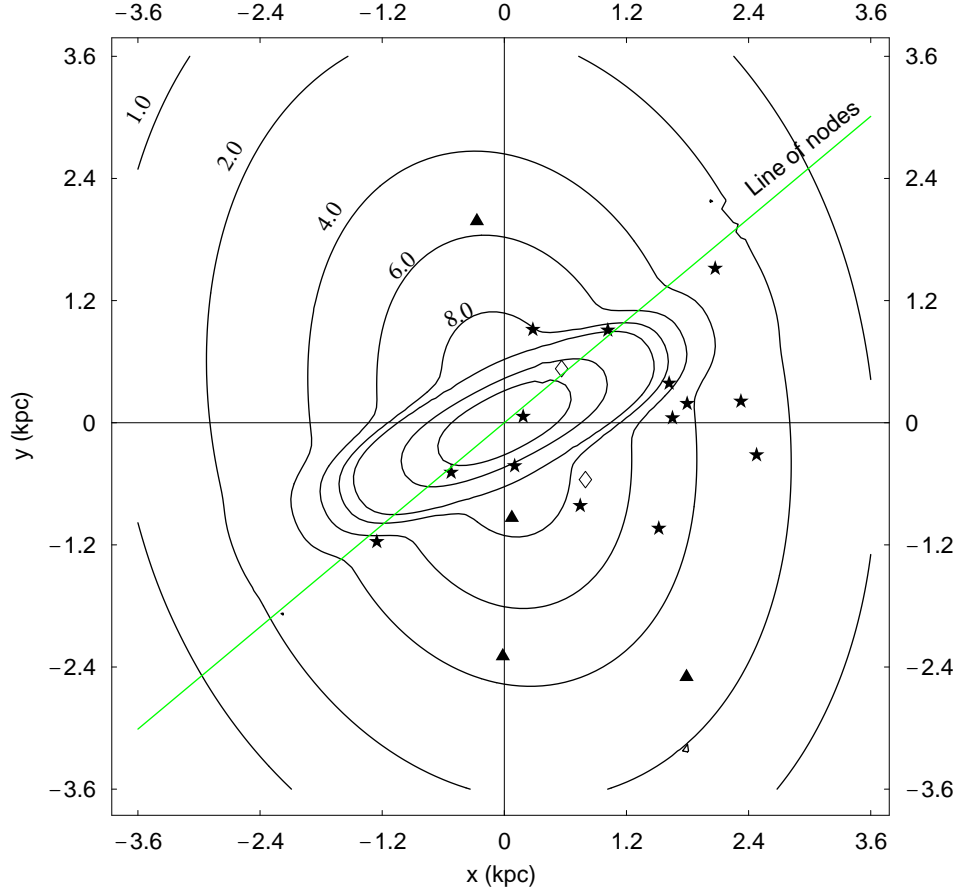


Figure 1. Projection on the sky plane ($x - y$ plane) of the column density of the LMC disk and bar. The numerical values on the contours are in $10^7 M_\odot \text{kpc}^{-2}$ units. The three innermost contours correspond to $10, 20$ and $30 \times 10^7 M_\odot \text{kpc}^{-2}$. The locations of the MACHO (black stars and empty diamonds) and EROS (triangles) microlensing candidates are also shown.

ρ_l denotes the mass density of the lenses, ρ_s the mass density of the sources, D_{ol} and D_{os} , respectively, the distance observer-lens and observer-source.

In Fig. 2 we report the optical depth contour maps for lenses belonging to the halo of LMC in the case of spherical model in the hypothesis that all the LMC dark halo consists of compact lenses. The ellipsoidal model leads to similar results⁸. A striking feature of the map is the strong near-far asymmetry.

For the spherical model, the maximum value of the optical depth, $\tau_{\text{max},s} \simeq 8.05 \times 10^{-8}$, is assumed in a point falling in the field number 13, belonging to the fourth quadrant, at a distance of $\simeq 1.27$ kpc from the center. The value in the point symmetrical with respect to the center, belonging to the second quadrant and

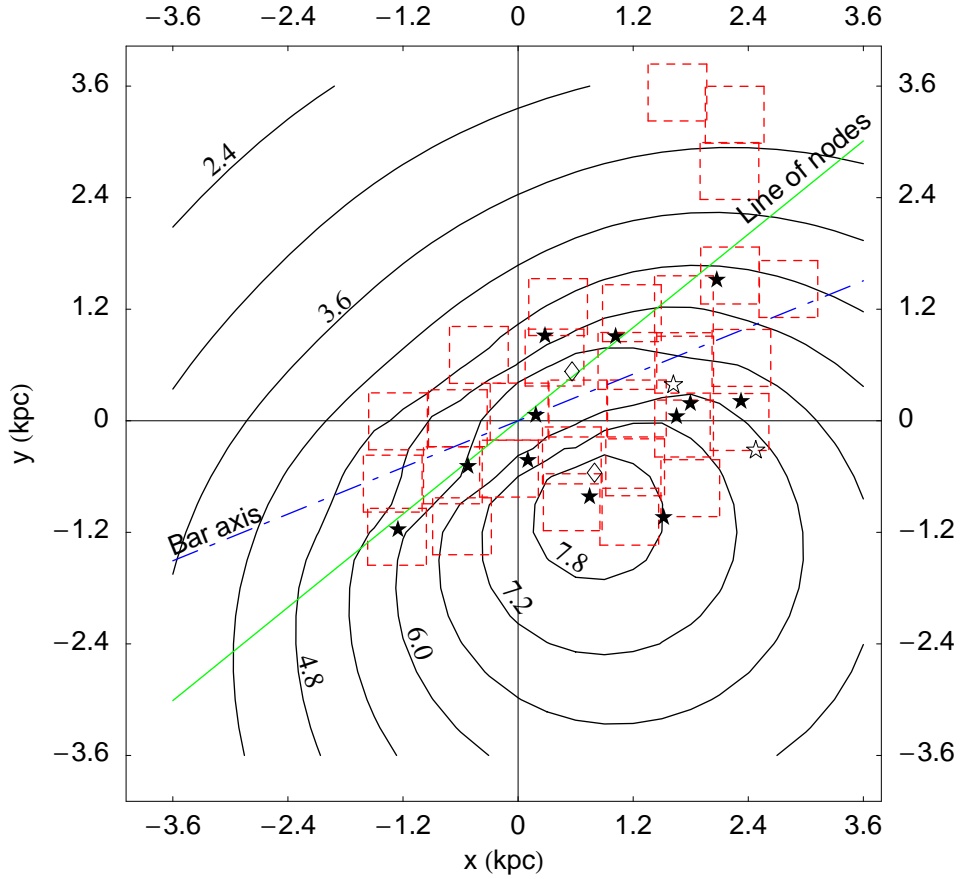


Figure 2. Spherical halo model: contour map of the optical depth for lenses in the LMC halo. The locations of the MACHO fields and of the microlensing candidates are also shown. The numerical values are in 10^{-8} units.

falling about at the upward left corner of the field 82, is $\tau_S \simeq 4.30 \times 10^{-8}$. The increment of the optical depth is of the order of $\approx 87\%$, moving from the nearer to the farther fields.

In Fig. 3 we report the optical depth contour map for self-lensing, i. e. for events where both the sources and the lenses belong to the disk and/or to the bulge of LMC. As expected, there is almost no near-far asymmetry and the maximum value of the optical depth, $\tau_{\max} \simeq 4.80 \times 10^{-8}$, is reached in the center of LMC. The optical depth then rapidly decreases, when moving, for instance, along a line going through the center and perpendicular to the minor axis of the elliptical disk, that coincides also with the major axis of the bar. In a range of about only 0.80 kpc

the optical depth quickly falls to $\tau \simeq 2 \times 10^{-8}$, and afterwards it decreases slowly to lower values.

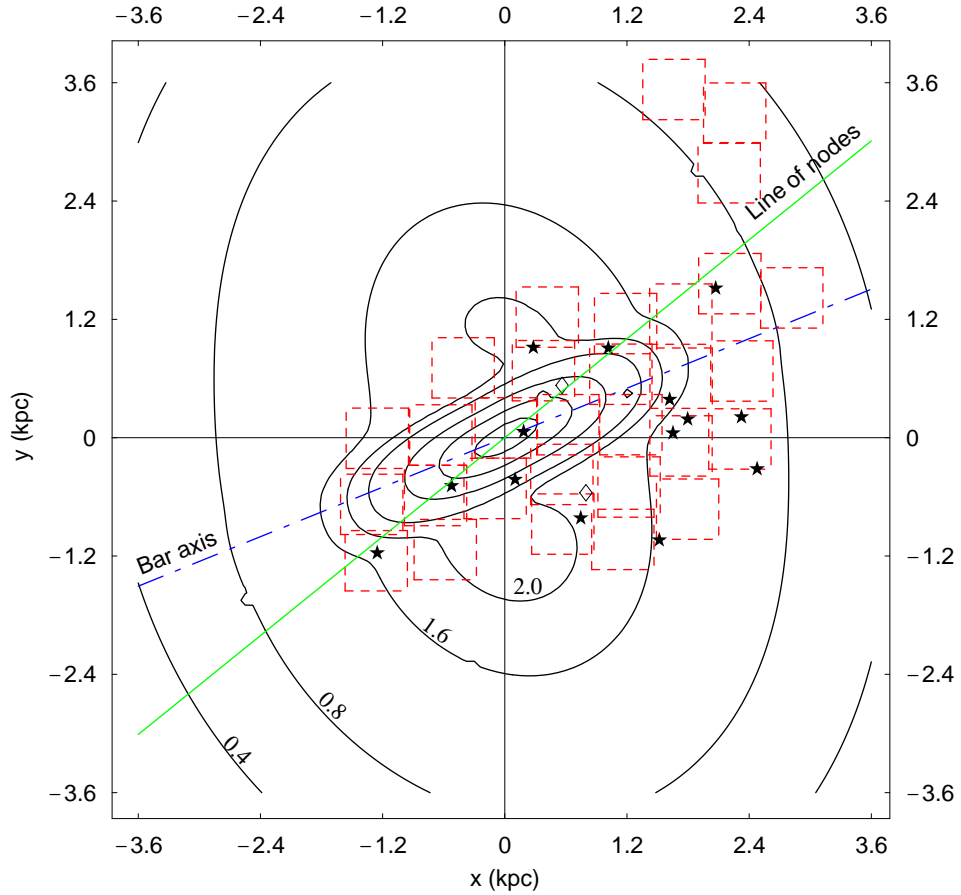


Figure 3. Contour map of the optical depth for self-lensing. The locations of the MACHO fields and of the microlensing candidates are also shown. The numerical values are in 10^{-8} units. The innermost contours correspond to values 2.4×10^{-8} , 3.2×10^{-8} , 4.0×10^{-8} and 4.6×10^{-8} respectively.

4. Self-lensing event rate

An important quantity, useful for the physical interpretation of microlensing events, is the distribution $\frac{d\Gamma}{dT_E}$, the differential rate of microlensing events with respect to the Einstein time T_E . In particular it allows us to estimate the expected typical duration and their expected number. We evaluated the microlensing rate in the

self-lensing configuration, i. e. lenses and sources both in the disk and/or in the bar of LMC. We have taken into account the transverse motion of the Sun and of the source stars. We assumed that, to an observer comoving with the LMC center, the velocity distribution of the source stars and lenses have a Maxwellian profile, with spherical symmetry.

In the picture of van der Marel et al. within a distance of about 3 kpc from the center of LMC, the velocity dispersion (evaluated for carbon stars) along the line of sight can be considered constant, $\sigma_{\text{los}} = 20.2 \pm .5$ km/s. Most of the fields of the MACHO collaboration fall within this radius and, furthermore, self-lensing events are in any case expected to happen in this inner part of LMC. Therefore, we adopted this value, even if we are aware that the velocity dispersion of different stellar populations in the LMC varies in a wide range, according to the age of the stellar population: $\simeq 6$ km/s for the youngest population, until $\simeq 30$ km/s for the older ones¹⁵.

We need now to specify the form of the number density. Assuming that the mass distribution of the lenses is independent of their position¹⁶ in LMC (*factorization hypothesis*), the lens number density per unit mass is given by

$$\frac{dn_l}{d\mu} = \frac{\rho_d + \rho_b}{M_\odot} \frac{dn_0}{d\mu}, \quad (6)$$

where we use $\frac{dn_0}{d\mu}$ as given in Chabrier¹⁷ ($\mu = M/M_\odot$). We consider both the power law and the exponential initial mass functions^a. However, we find that our results do not depend strongly on that choice and hereafter, we will discuss the results we obtain by using the exponential IMF only.

Let us note that, considering the experimental conditions for the observations of the MACHO team, we use as range for the lens masses $0.08 \leq \mu \leq 1.5$. The lower limit is fixed by the fact that the lens must be a star in LMC, while the upper limit is fixed by the requirement that the lenses are not resolved stars^b.

We compute the “field exposure”, E_{field} , defined, as in Alcock et al. ¹, as the product of the number of distinct light curves per field by the relevant time span, paying attention to eliminate the field overlaps; moreover we calculate the distribution $\frac{d\Gamma}{dT_E}$ along the line of sight pointing towards the center of each field. In this way we obtain the number of expected events for self-lensing, field by field, given by

$$N_{\text{SL,field}} = E_{\text{field}} \int_0^\infty \frac{d\Gamma}{dT_E} E(T_E) dT_E, \quad (7)$$

where $E(T_E)$ is the detection efficiency.

Summing over all fields we find that the expected total number of self-lensing events is ~ 1.2 , while we would get ~ 1.3 with the the double power law IMF;

^aWe have used the same normalization as in Jetzer et al. ⁷ with the mass varying in the range 0.08 to $10 M_\odot$.

^bWe have checked that the results are insensitive to the precise upper limit value.

in both cases altogether 1-2 events⁸. Clearly, taking also into account the uncertainties in the parameter used following the van der Marel model for the LMC the actual number could also be somewhat higher but hardly more than our upper limit estimate of about 3-4 events given in⁷.

4.1. *Self-lensing events discrimination*

It turns out that, in the framework of the LMC geometrical structure and dynamics outlined above, a suitable statistical analysis allows us to exclude from the self-lensing population a large subset of the detected events. To this purpose, assuming all the 14 events as self-lensing, we study the scatter plots correlating the self-lensing expected values of some meaningful microlensing variables with the measured Einstein time or with the self-lensing optical depth. In this way we can show that a large subset of events is clearly incompatible with the self-lensing hypothesis.

We have calculated the self-lensing distributions $\left(\frac{d\Gamma}{dT_E}\right)_{\varepsilon}$ of the rate of microlensing events with respect to the Einstein time T_E , along the lines of sight towards the 14 events found by the MACHO collaboration, in the case of a Chabrier exponential type IMF. With these distributions we have calculated the modal $T_{E,mod}$, the median $T_{E,50\%}$ and the average $\langle T_E \rangle$ values of the Einstein time.

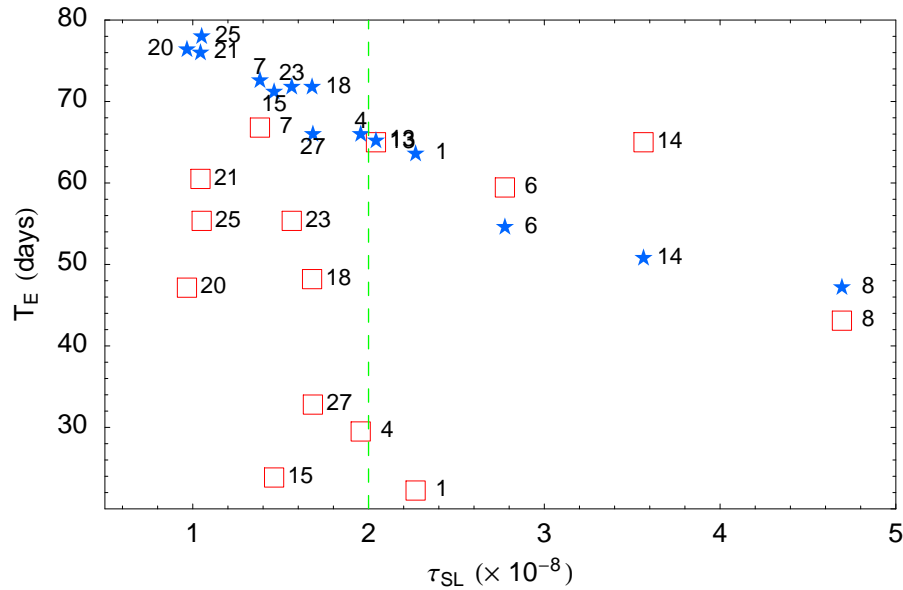


Figure 4. Scatter plot of the observed (empty boxes) values of the Einstein time and of the expected values of the median $T_{E,50\%}$ (filled stars), with respect to the self-lensing optical depth evaluated along the directions of the events.

In Fig. 4 we report on the y -axis the observed values of T_E (empty boxes)

as well as the expected values for self-lensing of the *median* $T_{E,50\%}$ (filled stars) evaluated *along the directions of the events*. On the x -axis we report the value of the self-lensing optical depth calculated towards the event position; the optical depth is growing going from the outer regions towards the center of LMC according to the contour lines shown in Fig. 3. An interesting feature emerging clearly is the *decreasing* trend of the expected values of the median $T_{E,50\%}$, going from the outside fields with low values of τ_{SL} towards the central fields with higher values of τ_{SL} . The variation of the stellar number density and the flaring of the LMC disk certainly contributes to explain this behaviour.

We now tentatively identify two subsets of events: the nine falling outside the contour line $\tau_{SL} = 2 \times 10^{-8}$ of Fig. 3 and the five falling inside. In the framework of van der Marel et al. LMC geometry, this contour line includes almost fully the LMC bar and two ear shaped inner regions of the disk, where we expect self-lensing events to be located with higher probability.

We note that, at glance, the two clusters have a clear-cut different collective behaviour: the measured Einstein times of the first 9 points fluctuate around a median value of 48 days, very far from the expected values of the median T_E , ranging from 66 days to 78 days, with an average value of 72 days. On the contrary, for the last 5 points, the measured Einstein times fluctuate around a median value of 59 days, very near to the average value 56 days of the expected medians, ranging from 47 days to 65 days. Let us note, also, the somewhat peculiar position of the event LMC-1, with a very low value of the observed T_E ; most probably this event is homogeneous to the set at left of the vertical line in Fig. 4 and it has to be included in that cluster.

This plot gives a first clear evidence that, in the framework of van der Marel et al. LMC geometry, the self-lensing events have to be searched among the cluster of events with $\tau_{SL} > 2 \times 10^{-8}$, and at the same time that the cluster of the 9 events including LMC-1 belongs, very probably, to a different population.

Moreover, when looking at the spatial distribution of the events one sees a clear near-far asymmetry in the van der Marel geometry; they are concentrated along the extension of the bar and in the south-west side of LMC. Indeed, we have performed a statistical analysis of the spatial distribution of the events, which clearly shows that the observed asymmetry is greater than the one expected on the basis of the observational strategy⁸.

5. Conclusions

We have presented the results of microlensing survey towards LMC by using the new picture of LMC given by van der Marel et al.¹². One interesting feature, that clearly emerges in this framework by studying the microlensing signature we expect to find, is an evident near-far asymmetry of the optical depth for lenses located in the LMC halo. Indeed, similarly to the case of M31^{18,19}, and as first pointed out by Gould²⁰, since the LMC disk is inclined, the optical depth is higher along

lines of sight passing through larger portions of the LMC halo. Such an asymmetry is not expected, on the contrary, for a self-lensing population of events. What we show is that, indeed, a spatial asymmetry that goes beyond the one expected from the observational strategy alone, and that is coherent with that expected because of the inclination of the LMC disk, is actually present. With the care suggested by the small number of detected events on which this analysis is based, this can be looked at, as yet observed by Gould²⁰, as a signature of the presence of an extended halo around LMC.

As already remarked, any spatial asymmetry is *not* expected for a self-lensing population of events, so that what emerges from this analysis can be considered as an argument to exclude it.

Furthermore, keeping in mind the observation²¹ that the timescale distribution of the events and their spatial variation across the LMC disk offers possibilities of identifying the dominant lens population, we have carefully characterized the ensemble of observed events under the hypothesis that all of them do belong to the self-lensing population. Through this analysis we have been able to identify a large subset of events that can not be accounted as part of this population. Again, the small amount of events at disposal does not yet allow us to draw sharp conclusions, although, the various arguments mentioned above are all consistent among them and converge quite clearly in the direction of excluding self-lensing as being the major cause for the events.

Once more observations will be available, as will hopefully be the case with the SuperMacho experiment under way²², the use of the above outlined methods can bring to a definitive answer to the problem of the location of the MACHOs and thus also to their nature.

References

1. Alcock, C., Allsman, R.A., Alves, D.R., et al. 2000a, ApJ **542**, 281
2. Milsztajn, A., & Lasserre, A. 2001, Nucl. Phys. B Proc. Sup. **91**, 413
3. Sahu, K.C. 1994, PASP **106**, 942
4. Aubourg, E., Palanque-Delabrouille, N., Salati, P., et al. 1999, A&A **347**, 850
5. Evans N. W., Gyuk, G., Turner M. S. & Binney J. J. 1998, ApJ **501**, L45
6. Zhao, H.S., & Evans, N.W. 2000, ApJ **545**, L35
7. Jetzer, Ph., Mancini, L. & Scarpetta, G. 2002, A&A **393**, 129
8. Mancini, L., Calchi Novati, S., Jetzer, Ph. & Scarpetta G. 2004, to appear in A&A
9. Alcock, C., Allsman, R.A., Alves, D.R., et al. 2000b, ApJ **541**, 270
10. Alcock, C., Allsman, R.A., Alves, D.R., et al. 2001b, ApJ **552**, 259
11. Alcock, C., Allsman, R.A., Alves, D.R., et al. 2001c, ApJ **552**, 582
12. van der Marel, R.P., & Cioni, M.R. 2001, AJ **122**, 1807
13. van der Marel, R.P. 2001, AJ **122**, 1827
14. van der Marel, R.P., Alves, D.R., Hardy, E., & Suntzeff, N.B. 2002, AJ **124**, 2639
15. Gyuk, G., Dalal, N. & Griest, K. 2000, ApJ **535**, 90
16. De Ríjula, A., Jetzer, Ph., & Massó, E. 1991, MNRAS **250**, 348
17. Chabrier, G. 2001, ApJ **554**, 1274

18. Crotts, A.P.S. 1992, *ApJ* **399**, L43
19. Jetzer, Ph. 1994, *A&A* **286**, 426
20. Gould, A. 1993, *ApJ* **404**, 451
21. Evans, N.W., & Kerins, E. 2000, *ApJ* **529**, 917
22. Stubbs, C. W., Rest, A., Miceli, A., et al. 2002, *BAAS* **201**, #78.07